



PAPER • OPEN ACCESS

Experimental verification of the inertial theorem control protocols

To cite this article: Chang-Kang Hu *et al* 2021 *New J. Phys.* **23** 093048

View the [article online](#) for updates and enhancements.

You may also like

- [Creation of electrical knots and observation of DNA topology](#)
Tian Chen, Xingen Zheng, Qingsong Pei et al.
- [A new self-filling mechanism of band gap in magnetically doped topological surface states: spin-flipping inelastic scattering](#)
Rui-Qiang Wang, Shi-Han Zheng and Mou Yang
- [Total nuclear reaction cross-section database for radiation protection in space and heavy-ion therapy applications](#)
F Luoni, F Horst, C A Reidel et al.



PAPER

Experimental verification of the inertial theorem control protocols

OPEN ACCESS

RECEIVED
27 April 2021REVISED
12 July 2021ACCEPTED FOR PUBLICATION
15 September 2021PUBLISHED
11 October 2021

Original content from
this work may be used
under the terms of the
[Creative Commons
Attribution 4.0 licence](#).

Any further distribution
of this work must
maintain attribution to
the author(s) and the
title of the work, journal
citation and DOI.



Chang-Kang Hu^{1,2,7}, Roie Dann^{3,4,7} , Jin-Ming Cui^{1,2} , Yun-Feng Huang^{1,2},
Chuan-Feng Li^{1,2} , Guang-Can Guo^{1,2}, Alan C. Santos^{5,6} and Ronnie Kosloff^{3,4,*}

¹ CAS Key Laboratory of Quantum Information, University of Science and Technology of China, Hefei 230026, People's Republic of China

² CAS Center For Excellence in Quantum Information and Quantum Physics, University of Science and Technology of China, Hefei 230026, People's Republic of China

³ The Institute of Chemistry, The Hebrew University of Jerusalem, Jerusalem 9190401, Israel

⁴ Kavli Institute for Theoretical Physics, University of California, Santa Barbara, CA 93106, United States of America

⁵ Instituto de Física, Universidade Federal Fluminense, Av. Gal. Milton Tavares de Souza s/n, Gragoatá, 24210-346 Niterói, Rio de Janeiro, Brazil

⁶ Departamento de Física, Universidade Federal de São Carlos, Rodovia Washington Luís, km 235 - SP-310, 13565-905 São Carlos, SP, Brazil

* Author to whom any correspondence should be addressed.

⁷ These authors contribute equally to this work.

E-mail: roie.dann@mail.huji.ac.il, jmcai@ustc.edu.cn, hyf@ustc.edu.cn, cffi@ustc.edu.cn,
ac_santos@df.ufscar.br and ronnie@fh.huji.ac.il

Keywords: quantum control, inertial theorem, trapped ytterbium

Abstract

An experiment based on a trapped ytterbium ion validates the inertial theorem for the $SU(2)$ algebra. The qubit is encoded within the hyperfine states of the atom and controlled by RF fields. The inertial theorem generates analytical solutions for non-adiabatically driven systems that are 'accelerated' slowly, bridging the gap between the sudden and adiabatic limits. These solutions are shown to be stable to small deviations, both experimentally and theoretically. By encoding a two-level system into hyperfine structure of a trapped ytterbium, we explore the high control over the system dynamics in order to validate range of applicability of the inertial theorem in our system. For large deviations from the inertial condition, the experimental results show that the phase remains accurate while the amplitude diverges, so the inertial theorem has good robustness in the phase estimate. As a result, we experimentally showed that the inertial solutions pave the way to rapid quantum control of closed, as well as open quantum systems.

1. Introduction

Progress in contemporary quantum technology requires precise control of quantum dynamics [1–20]. To answer the demand, a 'universal' vocabulary of control techniques has emerged. They have been applied across a broad range of experimental platforms, such as NV-centers [21–23], trapped ions [2, 24, 25], and Josephson devices [26–28]. These techniques are encapsulated within the theoretical framework of quantum control theory [1, 29–31].

This theory formulates the control problem by addressing three main topics:

- (a) Controllability, i.e., the conditions on the dynamics that allow obtaining the objective.
- (b) Constructive mechanisms of control, the problem of synthesis.
- (c) Optimal control strategies and quantum speed limits.

The first issue controllability of unitary dynamics of closed quantum system has been formulated employing Lie algebra techniques [30, 32, 33]. In this case, the Hamiltonian of the system is separated into

drift and control terms

$$\hat{H}(t) = \hat{H}_0 + \sum_j g_j(t) \hat{G}_j, \quad (1)$$

where \hat{H}_0 is the free system Hamiltonian, $\{g_j(t)\}$ are the control fields and $\{\hat{G}_j\}$ are control operators. The system is unitary controllable provided that the Lie algebra, spanned by the nested commutators of \hat{H}_0 and \hat{G}_j , is full rank [30, 32–34].

When addressing the quantum control challenge, it is reassuring that a solution exists, nevertheless, the practical problem of finding a control protocol has not been solved. For this task a pragmatic approach has been developed, formulating the control problem as an optimization problem, leading to optimal control theory [1, 35–37]. This approach has achieved significant success in solving specific control problems. However, the drawback is that obtaining the control protocol relies on a specific numerical scheme which might be difficult to obtain and to generalize [38].

The present study is devoted to the experimental study of constructive mechanisms of control. Experimental realization based on quantum control impose additional requirements: (i) the control protocol should be robust under experimental errors and (ii) the mechanism should be clear and simple to generalize. These considerations have singled out the adiabatic protocols which have dominated the control field, across all platforms [39, 40]. Adiabatic methods are based on the adiabatic theorem which loosely states that the system will follow an eigenvalue of the instantaneous Hamiltonian, provided that the change in time is slow relative to the time associated with the relevant energy gaps [41, 42]. The fact that the Hamiltonian is an invariant of the dynamics enables a simple implementation of the control protocol by choosing the initial and final states as eigenstates of the Hamiltonian. The adiabatic condition on the change in the Hamiltonian will then generate the desired transition. The robustness of such a protocol stems from the redundancy in the intermediate Hamiltonian, which allow variations in the protocol, provided the changes are sufficiently slow. This implies that the adiabatic protocol timescale is large relative to the system free dynamics. The relatively long protocol durations mean that the adiabatic protocols become prone to environmental noise. This fact is one of the major disadvantages of the adiabatic method.

The present study is devoted to an experimental exploration for rapid alternative control protocol, which are based on the inertial theorem [43]. Such protocols are termed inertial protocols and are based on time-dependent invariants of the dynamics, beyond the adiabatic approximation. They serve as natural replacements of the instantaneous Hamiltonian of the adiabatic protocols. The inertial theorem follow a similar procedure as the standard adiabatic theorem [44]. As a consequence, the inertial and adiabatic solutions share a similar structure, which implies that the positive features of robustness and simplicity are maintained without paying the price of long timescales.

The experimental demonstration of the theory is based on the $SU(2)$ algebra, which is realized by $^{171}\text{Yb}^+$ ion confined in a Paul trap [45]. Trapped ions are characterized by long coherence times, multiple degrees of freedom such as internal and external states, both of which are well controlled. Therefore it is one of the leading platforms employed to realize quantum information processing. Specifically the ytterbium ion is well suited to demonstrate of the inertial theorem for the following reasons. The ion can be efficiently cooled by lasers to a single quantum state. In addition, an effective two level system can be identified and manipulated by a RF pulse generator, which can produce controlled pulses. These pulses allow realizing a variety of inertial protocols with very high fidelity. Finally, an efficient readout is obtained by fluorescence detection. The system is well isolated and the typical timescale of dissipation is much longer than the protocol time.

2. Inertial theory and solution

For a quantum control scheme to be generic, it has to rely on simple principles that apply across many platforms. The control procedure requires the formulation of a dynamical map Λ_t from an initial state $\hat{\rho}(0)$, to the final state $\hat{\rho}(t) = \Lambda_t \hat{\rho}(0) = \hat{U} \hat{\rho}(0) \hat{U}^\dagger$. The dynamical map is generated by the control Hamiltonian equation (1):

$$i \frac{\partial}{\partial t} \hat{U}(t) = \hat{H}(t) \hat{U}(t) \quad \text{with} \quad \hat{U}(0) = \hat{I}, \quad (2)$$

where the convention $\hbar = 1$ is used throughout this paper.

The major obstacle in generating such a map from a time-dependent control Hamiltonian is the time-ordering operation, resulting from the fact that $[\hat{H}(t), \hat{H}(t')] \neq 0$. The adiabatic control circumvents this problem by employing a slow drive $g_j(t)$, allowing an approximate description in terms of the instantaneous eigenstates [42, 46–49]. At the other extreme, the sudden limit, the control is so fast that it

overshadows the dynamics generated by the drift Hamiltonian \hat{H}_0 . This leads to an instantaneous change of the Hamiltonian, while leaving the system's state unaffected.

The inertial dynamics and control paradigm serves as a compromise between the two extremes. It is based on the inertial theorem [43], which introduces an explicit solution of the dynamical map Λ_t under certain restrictions. The theorem is formulated in Liouville space, a vector space of system operators $\{\hat{X}\}$, endowed with an inner product $(\hat{X}_i, \hat{X}_j) \equiv \text{tr}(\hat{X}_i^\dagger \hat{X}_j)$ [50–52]. In Liouville space, the system's dynamics are represented in terms of a basis of orthogonal operators $\{\hat{B}\}$, spanning the space. For example, the currently studied $SU(2)$ algebra can be completely characterized by a time-independent operator basis constructed from the Pauli operators $\{\hat{I}, \hat{\sigma}_x, \hat{\sigma}_y, \hat{\sigma}_z\}$. The chosen (ordered) operator basis then defines a state in Liouville space. Note, that a time-dependent operator basis can also be chosen, $\{\vec{v}(t)\} \equiv \{\hat{V}_1(t), \dots, \hat{V}_N(t)\}^T$, where N the Liouville space dimension, which corresponds to the square of the associated (wave-function) Hilbert space. The possibility for a time-dependent operator basis serves as a major component in the inertial theorem and construction of inertial solutions. The use of Liouville space is motivated by the dynamical framework of open quantum systems, which requires the description of the system by the density operator. Specifically, this will allow us to describe the influence of external noise on the control, see discussion after equation (35).

In non-technical terms the theorem states the following, a physical system remains in its eigenoperators if a given perturbation changes inertially. This condition can be connected in certain cases to a slow acceleration of the perturbation and the existence of sufficient gaps between the eigenvalues of the eigenoperators.

The dynamics in Liouville space can be solved by substituting the chosen basis $\vec{v}(t)$ into the Heisenberg equation of motion,

$$\frac{d}{dt} \vec{v}^H(t) = \hat{U}^\dagger(t, 0) \left[\left(i [\hat{H}(t), \bullet] + \frac{\partial}{\partial t} \right) \vec{v}(t) \right] \hat{U}(t, 0), \quad (3)$$

where superscript H signifies that the operators are in the Heisenberg picture.

We next consider a finite time-dependent basis, forming a closed Lie algebra, this guarantees that equation (3) can be solved within the basis [53]. For a closed Lie algebra, equation (3) has the simple form

$$\frac{d}{dt} \vec{v}^H(t) = -i\mathcal{M}(t) \vec{v}^H(t), \quad (4)$$

where $\mathcal{M}(t)$ is a finite matrix with time-dependent elements and $\vec{v}(t)$ is a vector.⁸

The inertial solutions are obtained by searching for a driving protocol that allows solving equation (4) explicitly. These then enable extending the exact solutions for a broad range of protocols employing the inertial approximation. By choosing a unique driving protocol and the suitable time-dependent operator basis, the dynamical equation can be expressed as

$$\mathcal{M}(t) = \mathcal{P}(\vec{\chi}) \mathcal{D}(\vec{\chi}, \vec{\Omega}) \mathcal{P}^{-1}(\vec{\chi}). \quad (5)$$

Here, $\mathcal{P}(\vec{\chi})$ is an invertible matrix, which depends on the inertial coefficients $\{\chi_k\}$ (for conciseness they are expressed in terms of the vector $\vec{\chi} = \{\chi_1, \dots, \chi_K\}$), and $\mathcal{D} = \text{diag}(\lambda_1(\vec{\chi})\Omega_1(t), \dots, \lambda_N(\vec{\chi})\Omega_N(t))$ is a diagonal matrix, whose elements depend on time-dependent frequencies $\vec{\Omega}(t) = \{\Omega_1(t), \dots, \Omega_N(t)\}$, and coefficients $\{\lambda_k\}$. Such a time-dependent operator basis always exists, however, finding an analytical solution may be difficult and requires ingenuity, see [43] section V and [54] section VIII for further details.

Substituting the general decomposition equation (5) into the dynamical equation, equation (4) leads to an exact solution for $\vec{v}^H(t)$

$$\vec{v}^H(t) = \sum_{k=1}^{N^2} c_k \vec{F}_k(\vec{\chi}) e^{-i\lambda_k \theta_k(t)}, \quad (6)$$

where the scaled-time parameters are $\theta_k(t) = \int_0^t dt' \Omega_k(t')$ and $c_k = \sum_i \mathcal{P}_{ik}$ are constant coefficients. The Liouville vector \vec{F}_k corresponds to the eigenoperator $\hat{F}_k = \sum_i \mathcal{P}_{ki}^{-1} \hat{V}_i(0)$, where \mathcal{P}_{ik}^{-1} are elements of \mathcal{P}^{-1} and $\{\hat{V}_i(0)\}$ are the entities of the vector of operators $\vec{v}(0)$. For a Hermitian \mathcal{M} , the eigenvalues λ_k are either zero or are pairs with equal magnitude and opposite signs.

The solution (6) is exact, but is limited to protocols for which $\vec{\chi}$ is constant. This serves as a very severe constraint on the possible control protocols. However, the restriction can be loosened by utilizing the inertial theorem, which introduces approximate solutions for protocols with slowly varying $\vec{\chi}(t)$.

⁸ For the case of compact Lie algebras and unitary dynamics, \mathcal{M} is guaranteed to be Hermitian.

For a state \vec{v} , driven by an inertial protocol, the system's evolution is given by

$$\begin{aligned}\vec{v}^H(t) &= \sum_{k=1}^{N^2} c_k(\vec{\chi}(t)) e^{-i\int_0^t dt' \lambda_k \Omega_k} e^{i\phi_k(t)} \vec{F}_k(\vec{\chi}(t)) \\ &= \mathcal{P}(\vec{\chi}(t)) e^{-i\int_{\vec{\chi}(0)}^{\vec{\chi}(t)} \lambda_k(\theta'_k) d\theta'_k} \mathcal{P}^{-1}(\vec{\chi}(t)) \vec{v}^H(0),\end{aligned}\quad (7)$$

where the first exponent is determined by the dynamical phase and the second includes a new geometric phase

$$\phi_k(t) = i \int_{\vec{\chi}(0)}^{\vec{\chi}(t)} d\vec{\chi} \left(\vec{G}_k, \nabla_{\vec{\chi}} \vec{F}_k \right). \quad (8)$$

Here, \vec{G}_k are the bi-orthogonal partners of \vec{F}_k . The inertial solution is characterized by two timescales: the fast timescale is incorporated within the frequencies $\Omega_k(t)$, while the slow timescale is associated with the change in the inertial parameters $\chi_k(t)$.

The system's state follows the instantaneous solution determined by the instantaneous $\vec{\chi}(t)$ and phases, associated with the eigenvalues $\lambda_k \Omega_k$ and eigenoperators \vec{F}_k . We restrict the analysis to the case where $\lambda_k \Omega_k$ do not cross, hence, the spectrum of \mathcal{D} remains non-degenerate throughout the evolution. Substituting the inertial solution, equation (7), into equation (4) enables assessing the validity of the approximation in terms of the 'inertial parameter'

$$\Upsilon = \sum_{n,k} \left| \frac{\left(\vec{G}_k, \nabla_{\vec{\chi}} \mathcal{M} \vec{F}_n \right)}{(\lambda_n \Omega_n - \lambda_k \Omega_k)^2} \left(\frac{d\vec{\chi}}{dt} \right)^2 \right|. \quad (9)$$

This implies that the inertial solution, equation (7), remains valid when $\vec{\chi}$ follows a path in the parameter space of $\{\chi_k\}$, where the eigenvalues λ_k and λ_n are distinct [49].

Overall, the inertial solution is a linear combination of the instantaneous eigenoperators $\{\vec{F}_k\}$, and holds for slow variation of $\vec{\chi}$, i.e., $d\vec{\chi}/dt \ll 1$, $\Upsilon \ll 1$. Physically, the condition on $d\vec{\chi}/dt$, is associated with a slow 'adiabatic acceleration' of the driving [43]. In the adiabatic limit, decomposition equation (5) is satisfied instantaneously, where $\vec{\chi} \ll 1$, and the inertial solution converges to the adiabatic result.

The implications of the inertial solution equation (7), can be understood by considering the analogy with the adiabatic solution $|\psi_{\text{adi}}(t)\rangle = \sum_n c_n^{\text{adi}}(0) e^{i\theta_n^{\text{adi}}(t)} e^{i\phi_n^{\text{adi}}(t)} |n(t)\rangle$, where $|n(t)\rangle$ are the instantaneous eigenstates of the Hamiltonian, θ_n^{adi} and ϕ_n^{adi} are the adiabatic solution's dynamical and geometric phases, and $c_n^{\text{adi}}(0)$ are the coefficients of the initial state. The Hamiltonian in the adiabatic theorem plays similar role as the dynamical generator in Liouville space $\mathcal{M}(t)$ in the inertial solution, as a consequence, the Hamiltonian's instantaneous eigenstates are analogous to the eigenoperators $\{\vec{F}_k(\vec{\chi}(t))\}$. The analogy between $\hat{H}(t)$ and $\mathcal{M}(t)$ is not perfect, in the inertial theorem the eigenvalues of the dynamical generator are decomposed to fast $\{\Omega_k(t)\}$ and slow components $\{\lambda_k(t)\}$. Unlike the adiabatic theorem, this separation of timescales allows rapid changes in $\mathcal{M}(t)$, which is associated with a Hamiltonian that violates the adiabatic condition. The rapid degrees of freedom are incorporated within a scaled time $\int_0^t \Omega_k(\tau) d\tau$, which is specific to each eigenoperator (k -dependent) and determines the quality of the inertial approximation. Effectively, an inertial solution is valid when the dynamical generator in Liouville space changes slowly with respect to the scaled times, and there is a sufficient gap in the spectrum of the generator, see equation (9).

2.1. Inertial solution for an $SU(2)$ algebra

We will demonstrate the inertial solution in the context of the $SU(2)$ algebra. The simplest realization is by a two-level-system (TLS). In particular, the algebra represents the effective qubit in the ytterbium ion. For the demonstration, we choose a dynamical map Λ_t that varies the energy scale and controls the relation between energy and coherence in a non-periodic fashion. The control Hamiltonian is chosen as:

$$\hat{H}(t) = \frac{1}{2} (\omega(t) \hat{\sigma}_z + \epsilon(t) \hat{\sigma}_x), \quad (10)$$

where the control protocol are parameterized as follows

$$\begin{aligned}\omega(t) &= \Omega(t) \cos(\alpha(t)) \\ \epsilon(t) &= \Omega(t) \sin(\alpha(t))\end{aligned}\quad (11)$$

Here, the frequencies ω and ϵ are the detuning and Rabi frequency, respectively. As we shall see, in a single trapped ion system, the time-dependent functions $\omega(t)$ and $\epsilon(t)$ can be efficiently controlled by using the

detuning and field intensity of a driving microwave field. These define the generalized Rabi frequency $\Omega(t) \equiv \sqrt{\epsilon^2(t) + \omega^2(t)}$.

We choose a time-dependent operator basis which can factorize the equation of motion $\vec{v}^H(t) = \{\hat{H}(t), \hat{L}(t), \hat{C}(t), \hat{I}\}^T$, where

$$\begin{aligned}\hat{L}(t) &= (\epsilon(t) \hat{\sigma}_z - \omega(t) \hat{\sigma}_x) / 2 \\ \hat{C}(t) &= (\Omega(t) / 2) \hat{\sigma}_y,\end{aligned}\quad (12)$$

and \hat{I} is the identity operator.

Since \hat{I} is a constant of motion, a reduction to a 3×3 vector space in the basis $\{\hat{H}(t), \hat{L}(t), \hat{C}(t)\}$ is sufficient for the dynamical description. Following the general procedure, we calculate the dynamics of $\vec{v}^H(t)$, equation (3), to obtain a generator of the form

$$\mathcal{M}_{\text{TLS}}(t) = \Omega(t) \mathcal{B}(\mu). \quad (13)$$

with

$$\mathcal{B}(\mu) \equiv i \frac{\dot{\Omega}}{\Omega^2} \mathcal{I} + \mathcal{B}'(\mu), \quad (14)$$

and

$$\mathcal{B}'(\mu) \equiv i \begin{bmatrix} 0 & \mu & 0 \\ -\mu & 0 & 1 \\ 0 & -1 & 0 \end{bmatrix}. \quad (15)$$

We can now identify the inertial coefficient $\vec{\chi} = \chi = \mu$ with the adiabatic parameter of Hamiltonian, equation (10), it is defined as

$$|\mu(t)| \equiv \frac{\dot{\omega}\epsilon - \dot{\epsilon}\omega}{\Omega^3} \sim \sum_{n \neq m} \frac{|\langle E_m(t) | \dot{\hat{H}}(t) | E_n(t) \rangle|}{(E_m(t) - E_n(t))^2}. \quad (16)$$

Defining the scaled time $\theta(t) = \int_0^t \Omega(t') dt'$ and decomposing the system state as

$$\vec{v}^H(t) = \vec{u}^H(t) \exp \int_0^t \frac{\dot{\Omega}}{\Omega} dt' = \frac{\Omega(t)}{\Omega(0)} \vec{u}^H(t) \quad (17)$$

leads to a time-independent equation for $\vec{u}^H(\theta)$

$$\frac{d}{d\theta} \vec{u}^H(\theta) = \begin{bmatrix} 0 & \mu & 0 \\ -\mu & 0 & 1 \\ 0 & -1 & 0 \end{bmatrix} \vec{u}^H(\theta). \quad (18)$$

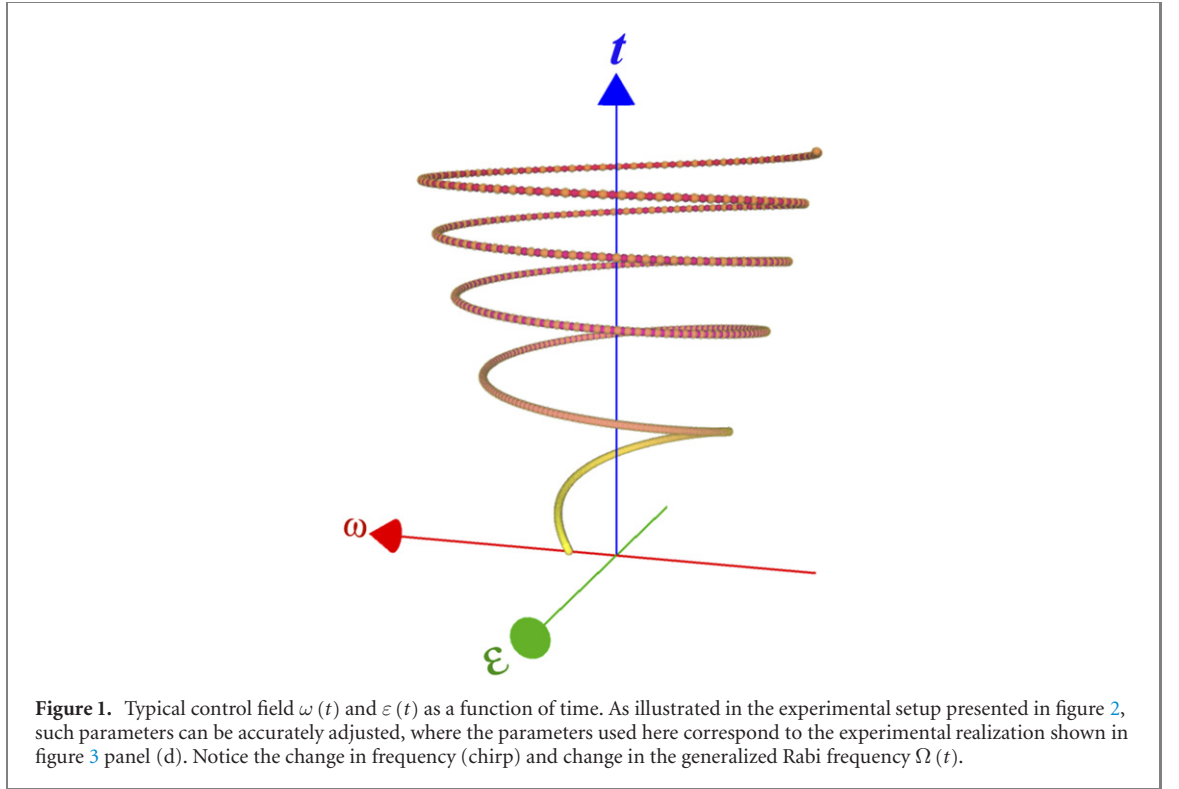
For a constant adiabatic parameter μ , we solve equation (18) by diagonalization and obtain a solution in terms of the basis of eigenoperators $\vec{F} = \{\hat{F}_1, \hat{F}_2, \hat{F}_3, \hat{I}\}^T$. The solution reads

$$\vec{F}(t) = e^{-i\mathcal{D}\theta(t)} \vec{F}(0), \quad (19)$$

where $\mathcal{D} = \text{diag}(0, \kappa, -\kappa, 0)$ with $\kappa = \sqrt{1 + \mu^2}$. The eigenoperators \hat{F}_k are associated with the eigenvectors of \mathcal{B}' . The eigenoperators are calculated with the help of the diagonalization matrix \mathcal{P} : $\vec{F}_i = \sum_j \mathcal{P}_{ij}^{-1} \vec{u}_j$. In the $\vec{v}(t) = \{\hat{H}(t), \hat{L}(t), \hat{C}(t), \hat{I}\}$ basis the eigenoperators can be written as:

$$\begin{aligned}\vec{F}_1 &= \frac{\mu}{\kappa^2} \{1, 0, \mu, 0\}^T \\ \vec{F}_2 &= \frac{1}{2\kappa^2} \{-\mu, -i\kappa, 1, 0\}^T \\ \vec{F}_3 &= \frac{1}{2\kappa^2} \{-\mu, i\kappa, 1, 0\}^T,\end{aligned}\quad (20)$$

with corresponding eigenvalues are $\lambda_1 = 0$, $\lambda_2 = \kappa$ and $\lambda_3 = -\kappa$. The vector \vec{F}_1 corresponds to a time dependent constant of motion i.e. $\langle \hat{F}_1(t) \rangle = \text{const}$, with $\hat{F}_1(t) = \frac{\mu}{\kappa^2} (\hat{H}(t) + \mu \hat{C}(t))$. Interestingly, the eigenstates of the $\hat{F}_1(t)$, $|\psi_{\pm}\rangle \propto \{\omega \pm \kappa\Omega, \epsilon + i\mu\Omega\}^T$, constitute dark states of the dynamics. Similar to an energy eigenstate they only accumulate a phase throughout the evolution. Any system observable can be expressed in terms of the eigenoperators $\{\hat{F}_k\}$, at initial time, and the exact evolution is then given by equation (19).



The exact solution relied on the condition of a constant adiabatic parameter, leading to the factorization equation (5). Such factorization enables employing the inertial theorem to extend the exact solution for a slow change in the adiabatic parameter ($\dot{\mu} \ll 1$), leading to an analogous equation to equation (7). Making use of equation (17) and the definition of \vec{F}_k equation (20), the solution of the $SU(2)$ dynamics becomes (the geometric phase vanishes in this case)

$$\vec{v}^H(t) = \frac{\Omega(t)}{\Omega(0)} \mathcal{P}(\mu(t)) e^{-i \int_0^t \mathcal{D}(\mu(t')) \Omega(t') dt'} \times \mathcal{P}^{-1}(\mu(t)) \vec{v}^H(0). \quad (21)$$

We experimentally verify the inertial solution by choosing a protocol associated with a linear change in the adiabatic parameter so that $\frac{d\mu}{dt} = \delta$

$$\mu(t) = \mu(0) + \delta \cdot t \quad (22)$$

and consider a linear chirp of the protocol frequencies

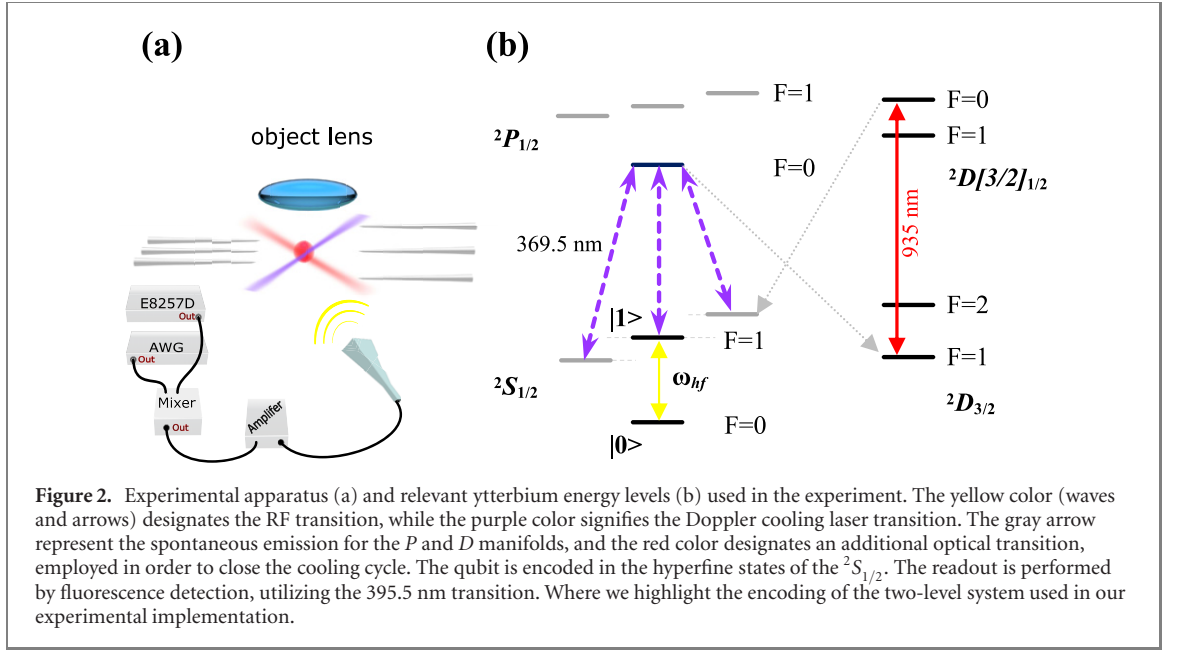
$$\alpha(t) = \alpha(0) + \gamma \cdot t. \quad (23)$$

equations (22) and (23) determine the Rabi frequency, by substituting this relation into equation (16) we obtain $\Omega(t) = -\frac{\alpha(0) + 2\gamma t}{\mu}$. For this protocol, the frequencies $\omega(t)$ and $\varepsilon(t)$ become

$$\begin{aligned} \omega(t) &= -\frac{(\alpha(0) + 2\gamma \cdot t)}{\mu(0) + \delta \cdot t} \cdot \cos((\alpha(0) + \gamma t) \cdot t) \\ \varepsilon(t) &= -\frac{(\alpha(0) + 2\gamma \cdot t)}{\mu(0) + \delta \cdot t} \cdot \sin((\alpha(0) + \gamma t) \cdot t) \end{aligned} \quad (24)$$

A typical control field corresponding to the frequencies $\omega(t)$ and $\varepsilon(t)$ is shown in figure 1, showing an evident change in frequency and amplitude.

The quality of the inertial approximation is directly connected to the parameter δ . For small $|\delta|$, the inertial approximation is satisfied and the inertial solution remains accurate. The accuracy of the inertial solution can be evaluated by utilizing the time-dependent control protocol, equation (24). We choose the initial condition $\vec{v}(0) = \{\hat{H}(0), 0, 0, 1\}$ which describes the system in the ground state ($\langle \hat{H}(0) \rangle = -\Omega(0)/2$). For these conditions, we compare the experimentally measured normalized energy, $\langle \hat{H}(t) \rangle / \langle \hat{H}(0) \rangle$, to the inertial solution, equation (21), and a converged numerical calculation of equation (4), which is generated by the Hamiltonian equation (10).



3. Experimental setup

The experimental analysis of the inertial solution employs a single ytterbium ion $^{171}\text{Yb}^+$, trapped in the six needles Paul trap, schematically shown in figure 2 panel (a). The TLS (qubit) used in our study is encoded in the hyperfine energy levels of the ion, represented as $|0\rangle \equiv ^2S_{1/2} |F=0, m_F=0\rangle$ and $|1\rangle \equiv ^2S_{1/2} |F=1, m_F=0\rangle$, with energies E_0 and E_1 , respectively, and where F denotes the total angular momentum of the atom and m_F is its projection along the quantization axis. In absence of an external field, the subspace $F=1$ is degenerate. Therefore, we apply an external static magnetic field \vec{B} with intensity 6.40 G to obtain a 8.9 MHz Zeeman structure splitting. This leads to the the desired TLS with a transition frequency given by $\omega_{\text{hf}} = 2\pi \times 12.642825$ GHz, see figure 2 panel (b).

We can define the bare Hamiltonian for our qubit as $H_0 = E_0 |0\rangle\langle 0| + E_1 |1\rangle\langle 1| = \hbar\omega_{\text{hf}}\sigma_z/2$, where $\sigma_z = |1\rangle\langle 1| - |0\rangle\langle 0|$ is the Pauli matrix. As schematically shown in figure 2, we can coherently manipulate the qubit by driving the system with an external magnetic field $\vec{B}_{\text{un}}(t) = \vec{B}_0 \cos(\omega t + \phi)$, one uses the dipole approximation to write the contribution of this interaction to energy of the system $H_1 = -\vec{\mu} \cdot \vec{B}_{\text{un}}(t)$, where $\vec{\mu} = \vec{\mu}_{01} |0\rangle\langle 1| + \vec{\mu}_{10} |1\rangle\langle 0|$ [55, 56]. For simplicity we assume $\vec{\mu}_{01} = \vec{\mu}_{10} = \vec{\mu}$, such that the control Hamiltonian reads $H_1(t) = -\vec{\mu} \cdot \vec{B}_0 \cos(\omega t + \phi)\sigma_x$. Then, the total driving Hamiltonian $H(t) = H_0 + H_1$ reads as

$$\hat{H}(t) = \frac{\hbar\omega_{\text{hf}}}{2}\sigma_z + \hbar\Omega_R \cos(\omega t + \phi)\sigma_x. \quad (25)$$

in which $\Omega_R \propto |\vec{B}_0|$. As aforementioned, in the rotating frame, the trapped ion driving Hamiltonian can be written as

$$\hat{H}_{\text{ion}} = \frac{\hbar\Delta}{2}\sigma_z + \frac{\hbar\Omega_R}{2} (\cos \phi \sigma_x + \sin \phi \sigma_y), \quad (26)$$

where $\Delta = \omega_{\text{hf}} - \omega$. Therefore, by putting the phase $\phi = 0$ and by controlling \vec{B}_0 and ω in time, it makes $\Delta = \omega(t)$ and $\Omega_R = \varepsilon(t)$, such that the above Hamiltonian is equivalent to the Hamiltonian given in equation (10), as considered in the previous section.

In our experiment, the driving magnetic field is generated by mixing a $2\pi \times 12.442$ GHz coherent local oscillator microwave and a programmable arbitrary waveform generator (AWG) signal, which is centered around $2\pi \times 200$ MHz [57, 58]. This microwave electronic setup enables to implement the components $\hat{\sigma}_z$ and $\hat{\sigma}_x$ of the Hamiltonian in equation (10), by simultaneous controlling the driving microwave phase, amplitude and frequency.

To initialize the experiment, first the motion of the ion is cooled by employing a 369.5 nm Doppler cooling laser beam, using the optical transition cycle $^2S_{1/2} \leftrightarrow ^2P_{1/2}$. During the transition cycle, there is a branching ratio R for population decay from $^2P_{1/2}$ state to the $^2D_{3/2}$ [59]. To send the system back to the cooling cycle, a light at 935.2 nm is used to promote transitions $^2D_{3/2} \leftrightarrow ^3D[3/2]_{1/2}$, where the system can quickly decay from $^3D[3/2]_{1/2}$ to $^2S_{1/2}$ (gray arrows in figure 2 panel (b)). After Doppler cooling, the system

is initialized in the $|0\rangle$ state with a standard optical pumping process. Utilizing the AWG, the time-frequency protocols of the inertial solutions are implemented.

The measurement procedure detects the population of the excited state of the qubit, using a fluorescence detection, induced by the 369.5 nm laser [57, 58]. Thus, detection of photons correspond to population in the bright state $|1\rangle$, while no photons signify population in the dark state $|0\rangle$, as shown in figure 2. The overall measurement fidelity is estimated to be 99.4% [57, 60]. This experiment is repeated many times, for different delay times and different inertial protocols. For each experimental protocol, the normalized energy as a function of time is evaluated $\langle \hat{H}(t) \rangle / \langle \hat{H}(0) \rangle$.

4. Results

The qubit's normalized energy as a function of time is shown in figure 3, comparing the experimental measurements (blue) to the analytical inertial solution (red) and an exact numerical simulation (black). As predicted by the inertial theorem, the dimensionless parameter $|\delta| = |d\mu/dt|$ plays a central role in the connection between experiment and theory, figure 3. Experiments with different δ (equation (24)) were realized to assess the range of validity of the inertial solution. The system evolution is theoretically predicted by numerically solving the Schrödinger equation, as shown with the black dotted curve in figure 3, while the experimental data is shown as blue symbols. For sake of comparison, we also present the expected solution for the inertial dynamics as derived from equation (21) (red full line in figure 3). In all the studied case we observe a good agreement between the theoretical, numerical and experimental data (black dotted curves fit very well the corresponding blue symbols). Given the high controllability of the dynamics, we can conclude that the theoretical and experimental results for small δ (see panel (c) and (d)), demonstrate the high accuracy of the inertial solution. In addition, it is worth highlighting that when $|\delta| = |d\mu/dt|$ is increased, we witness the breakdown of the inertial solution (panels (a), (b), (e) and (f)), since the deviations between the predicted normalized energy values of the inertial solution and the experimental results increase. The deviation is manifested by a difference in amplitude, while the phase of the inertial solution follows the exact simulation and experiment measurements, see section 4.1 for a detailed analysis.

Figure 4 shows the distance \mathcal{D} between the inertial solution and the exact numerical result as a function of δ and time. \mathcal{D} is defined as the Euclidean distance between the expectation values of the Liouville state vectors

$$\mathcal{D}(t) = \sqrt{\sum_{i=1}^3 (\langle v^i(t) \rangle - \langle v_{\text{num}}^i(t) \rangle)^2}, \quad (27)$$

where v^i and v_{num}^i are the i 'th component of \vec{v} (the inertial solution) and \vec{v}_{num} (the exact numerical solution). When μ varies slowly, ($\delta = -0.01$) the inertial solution remains exact, whereas for larger absolute values, the numerical and inertial solutions deviate linearly in δ and time. In figure 5, we present the inertial, numerical and adiabatic trajectories for $\delta = -0.01, -0.05$ in the $\langle \hat{H} \rangle, \langle \hat{L} \rangle, \langle \hat{C} \rangle$ space. This representation provides a complete description of the dynamics, demonstrating the large deviation between the adiabatic and inertial solutions.

4.1. Deviations from the exact solution

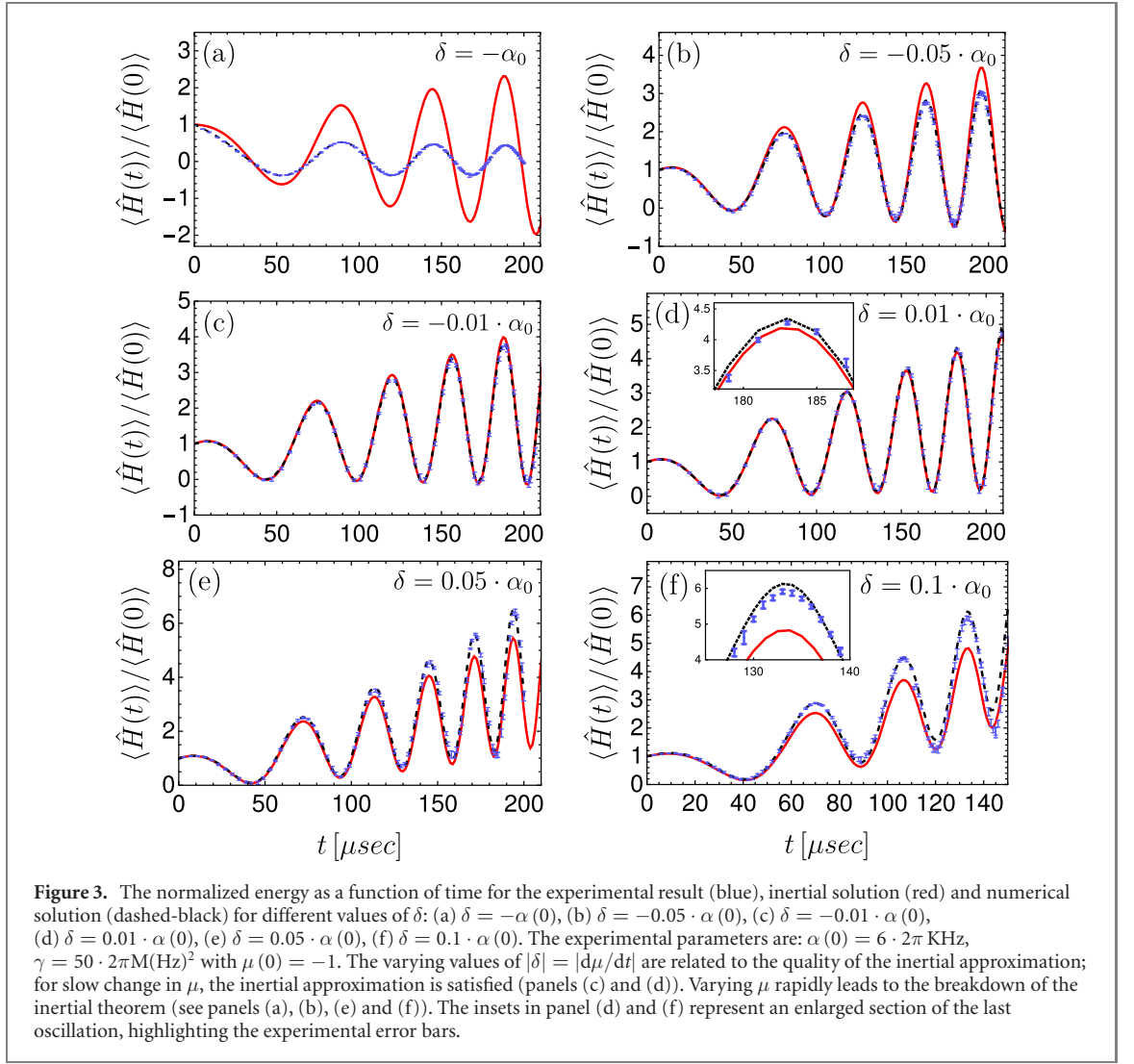
There are two major sources of deviation between the inertial solution and experimental results. The first is associated with the breakdown of the inertial solution and the second source concerns the inevitable experimental noise. Observing figure 3 we find that the major deviation between the theoretical and experimental results is in the amplitude of the energy oscillations, while the phase is not affected even for large $|\delta|$ (see for example panel (a) with $\delta = -\alpha(0)$). The amplitude of the inertial solution is determined by the real part of the eigenvalues of the propagator. These are dominated by the the general scaling associated with the change in the generalized Rabi frequency, see equation (17). The imaginary part of the eigenvalues determine the phase.

In order to rationalize the observed deviation we first analyze the correction terms to the inertial solution. Gathering equations (4), (13) and (17) we obtain

$$\frac{d\vec{u}^H(\theta)}{d\theta} = -i\mathcal{B}'(\mu(\theta))\vec{u}^H(\theta). \quad (28)$$

Next, we define the instantaneous diagonalizing matrix of $\mathcal{B}'(\mu)$, satisfying $\mathcal{P}^{-1}(\mu)\mathcal{B}'(\mu)\mathcal{P}(\mu) = \mathcal{D}(\mu)$ and the vector $\vec{w}^H(\theta) = \mathcal{P}^{-1}(\mu)\vec{u}^H(\theta)$. The dynamics of $\vec{w}^H(\theta)$ are given by

$$\frac{d\vec{w}(\theta)}{d\theta} = -i\mathcal{D}\vec{w}(\theta) + \mathcal{O}\vec{w}(\theta), \quad (29)$$



where $\mathcal{O} = -\mathcal{P}^{-1} \frac{d\mathcal{P}}{d\theta}$. For the studied model the diagonalizing matrix of $\mathcal{B}'(\mu)$, equation (15), obtains the form

$$\mathcal{P} = \frac{1}{2\kappa^2} \begin{pmatrix} 1 & -\mu & -\mu \\ \mu & i\kappa & -i\kappa \\ 1 & 1 & 1 \end{pmatrix} \quad (30)$$

For a slow change in μ , \mathcal{B}' and consequently \mathcal{P} vary slowly with respect to θ . This property allows neglecting the second term in equation (29), which is qualitatively similar to the inertial approximation. The deviations from the exact solution are reflected by the term $\mathcal{O}(\theta) = \mathcal{P}^{-1} \frac{d\mathcal{P}}{d\theta}$. Utilizing the identity $\frac{d\mathcal{P}}{d\theta} = \frac{1}{\Omega} \frac{d\mathcal{P}}{d\tau}$ we obtain

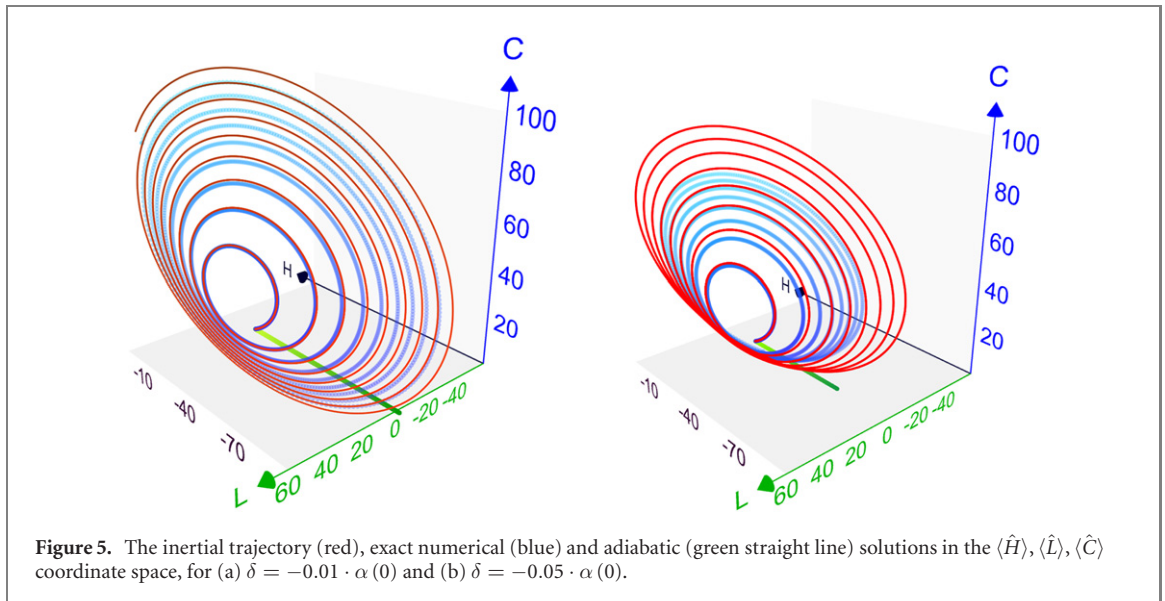
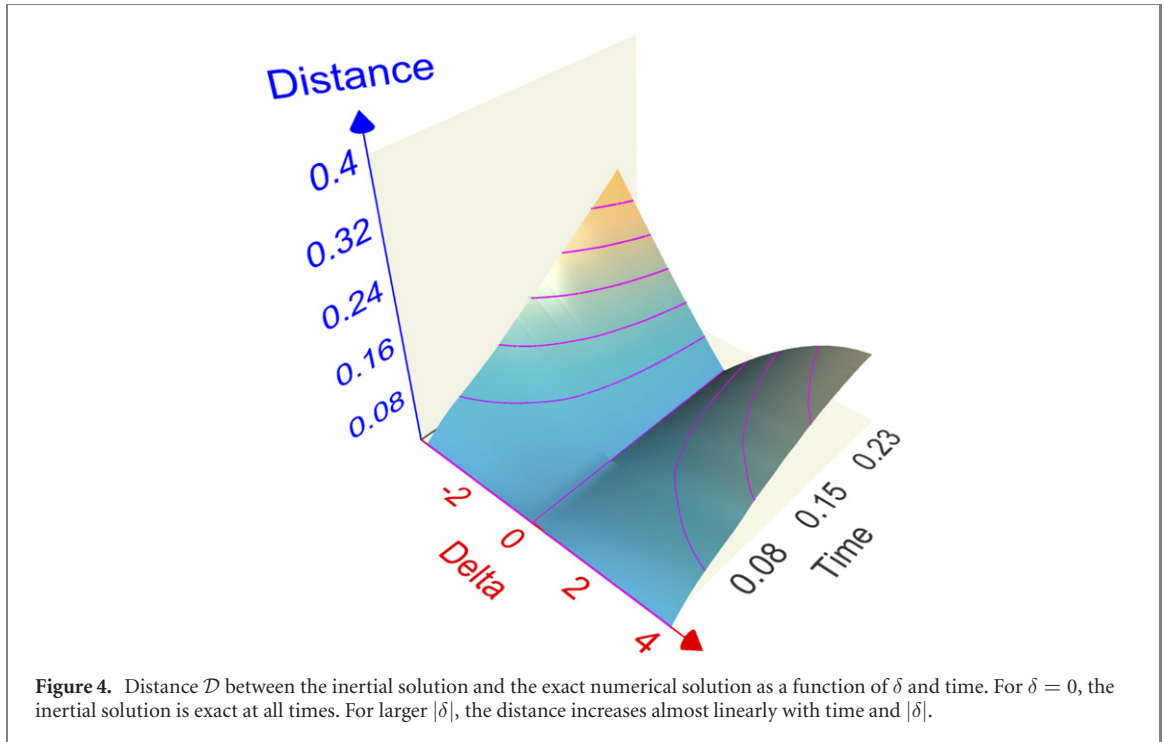
$$\mathcal{O} = \frac{2\mu}{1 + \mu^2} \frac{d\mu}{d\theta} \mathcal{I} + \mathcal{S}, \quad (31)$$

where

$$\mathcal{S} = \frac{\delta}{2\Omega\kappa^2} \begin{pmatrix} \frac{1}{\mu} & \mu & \mu \\ \frac{\mu}{1} & -\mu & 0 \\ -\frac{1}{2\mu} & 0 & -\mu \end{pmatrix}. \quad (32)$$

Solving the dynamics explicitly leads to

$$\vec{w}(\theta) = e^{(-i\mathcal{D} + \mathcal{O})\theta} \vec{w}(0). \quad (33)$$



Next, we utilize the Zassenhaus formula [61] to obtain a solution up to first order in θ

$$\vec{w}(\theta) \approx e^{-i\mathcal{D}\theta} e^{\mathcal{O}\theta} \vec{w}(0). \tag{34}$$

The correction term to the inertial solution has real eigenvalues, and therefore only influences the amplitude and not the phase. Thus, the phase of the inertial solution is not affected even when $|\mathrm{d}\mu/\mathrm{d}t| = |\delta|$ is large.

The second source of error is a consequence of experimental noise. We model this noise by a δ -correlated noise in the timing of the driving [62]. Such a process is equivalent to adding random noise to the generalized Rabi frequency $\Omega(t)$, equation (11). In the presence of such a noise the effective equation of motion includes double commutator in the operator generating the noise [63]. For timing noise this becomes [64]:

$$\frac{\mathrm{d}}{\mathrm{d}t} \vec{v}^H(t) = - [i\mathcal{M}(t) + \Gamma_n^2 \mathcal{M}^2(t)] \vec{v}^H(t), \tag{35}$$

where the double commutator is represented by \mathcal{M}^2 , and Γ_n is proportional to the noise amplitude. In this case, the noise has no effect on the eigenoperators with vanishing eigenvalues, \hat{F}_1 equation (20) (the

time-dependent constants of motion). The other two eigenvalues of the noise $\mathcal{M}^2(t)$ are real and therefore will only influence the amplitude of the signal. The experimental results shown in figure 3 in particular the insert of panel (d) and (f) corroborate this analysis.

5. Discussion

The purpose of this study was to establish experimentally a new family of inertial control protocols. These protocols are experimentally verified using a platform consisting of the hyperfine levels of an ytterbium ion $^{171}\text{Yb}^+$ in a Paul trap. This experimental platform is well suited for the evaluation due to its high fidelity. The high fidelity of both the control field and measurement allow direct comparison with the theoretical predictions. The inertial theorem provides a family of non-adiabatic protocols that bridge the gap between the sudden and adiabatic limits [43]. Specifically, we studied control of the $SU(2)$ Lie algebra, which constitutes the single qubit operations. We chose a protocol involving a chirp in frequency and change in the generalized Rabi frequency, associated with a linear change in the adiabatic parameter μ .

The experiments verify the theorem and the ability to perform inertial protocols. Moreover, as all experiments are influenced by various kinds of noise [65], the achieved accuracy confirms the robustness of the inertial solution. This conclusion is supported by theoretical simulations which verify that the solution is stable to small deviations and noise.

For a larger deviation from the inertial condition ($d\vec{\chi}/dt \rightarrow 1$) (figure 3 panels (a), (b), (e) and (f)), the error first appears in the amplitude, while the phase of the inertial solution is still accurate. We confirm this by analyzing a correction to the inertial solution. In the $SU(2)$ algebra, the first-order correction in θ to the phase vanishes (see the discussion following equation (31)). Incorporating the amplitude correction into the inertial solution can lead to higher accuracy. The phase information can be utilized for quantum parameter estimation [66] beyond the inertial limit.

Experimental validation of the inertial solution paves the way to rapid high-precision control. This control can be extended to *inertially* driven open systems [43], utilizing the non-adiabatic master equation [67]. Such control can regulate the system entropy [68, 69].

The present study constitutes a basic step in adding inertial control protocols to the family of constructive mechanisms of control. The experimental validation means that inertial protocols cross the barrier between a theoretical entity to laboratory use. Control based on the inertial theorem can be utilized in rapid applications of quantum information processing [65, 70–72] and sensing [73].

Acknowledgments

We thank KITP for their hospitality. This research was supported by the Adams Fellowship Program of the Israel Academy of Sciences and Humanities, the National Science Foundation under Grant No. NSF PHY-1748958 and the Israel Science Foundation Grant No. 2244/14, the National Key Research and Development Program of China (No. 2017YFA0304100), National Natural Science Foundation of China (Nos. 61327901, 61490711, 11774335, 11734015), the China Postdoctoral Science Foundation (Grant Nos. 2020M671861, 2021T140648), Anhui Initiative in Quantum Information Technologies (AHY070000, AHY020100), Anhui Provincial Natural Science Foundation (No. 1608085QA22), Key Research Program of Frontier Sciences, CAS (No. QYZDY-SSWSLH003), and the Fundamental Research Funds for the Central Universities (WK2470000026). ACS is supported by São Paulo Research Foundation (FAPESP) (Grant No 2019/22685-1). ACS acknowledges the partial financial support by the Coordenação de Aperfeiçoamento de Pessoal de Nível Superior and the Brazilian National Institute for Science and Technology of Quantum Information (INCT-IQ).

Data availability statement

The data that support the findings of this study are available upon reasonable request from the authors.

ORCID iDs

Roie Dann  <https://orcid.org/0000-0002-8883-790X>

Jin-Ming Cui  <https://orcid.org/0000-0002-5785-4248>

Chuan-Feng Li  <https://orcid.org/0000-0001-6815-8929>

Alan C. Santos  <https://orcid.org/0000-0002-6989-7958>

Ronnie Kosloff  <https://orcid.org/0000-0001-6201-2523>

References

- [1] Glaser S J *et al* 2015 Training Schrödinger's cat: quantum optimal control *Eur. Phys. J. D* **69** 1–24
- [2] Cirac J I and Zoller P 1995 Quantum computations with cold trapped ions *Phys. Rev. Lett.* **74** 4091
- [3] Monroe C, Meekhof D M, King B E, Itano W M and Wineland D J 1995 Demonstration of a fundamental quantum logic gate *Phys. Rev. Lett.* **75** 4714
- [4] Barreiro J T *et al* 2011 An open-system quantum simulator with trapped ions *Nature* **470** 486
- [5] Rosi S, Bernard A, Fabbri N, Fallani L, Fort C, Inguscio M, Calarco T and Montangero S 2013 Fast closed-loop optimal control of ultracold atoms in an optical lattice *Phys. Rev. A* **88** 021601
- [6] Mandel O, Greiner M, Widera A, Rom T, Hänsch T W and Bloch I 2003 Coherent transport of neutral atoms in spin-dependent optical lattice potentials *Phys. Rev. Lett.* **91** 010407
- [7] Bloch I, Dalibard J and Zwerger W 2008 Many-body physics with ultracold gases *Rev. Mod. Phys.* **80** 885
- [8] Jaksch D, Cirac J I, Zoller P, Rolston S L, Côté R and Lukin M D 2000 Fast quantum gates for neutral atoms *Phys. Rev. Lett.* **85** 2208
- [9] Duan L-M, Cirac J I and Zoller P 2001 Geometric manipulation of trapped ions for quantum computation *Science* **292** 1695–7
- [10] Jonathan D, Plenio M B and Knight P L 2000 Fast quantum gates for cold trapped ions *Phys. Rev. A* **62** 042307
- [11] Nielsen M A and Chuang I 2002 *Quantum Computation and Quantum Information* (Cambridge: Cambridge University Press)
- [12] Loss D and DiVincenzo D P 1998 Quantum computation with quantum dots *Phys. Rev. A* **57** 120
- [13] Kadowaki T and Nishimori H 1998 Quantum annealing in the transverse Ising model *Phys. Rev. E* **58** 5355
- [14] Finnila A B, Gomez M A, Sebenik C, Stenson C and Doll J D 1994 Quantum annealing: a new method for minimizing multidimensional functions *Chem. Phys. Lett.* **219** 343–8
- [15] Brooke J *et al* 1999 Quantum annealing of a disordered magnet *Science* **284** 779–81
- [16] Venegas-Andraca S E, Cruz-Santos W, McGeoch C and Lanzagorta M 2018 A cross-disciplinary introduction to quantum annealing-based algorithms *Contemp. Phys.* **59** 174–97
- [17] Johnson M W *et al* 2011 Quantum annealing with manufactured spins *Nature* **473** 194
- [18] Santoro G E, Martonak R, Tosatti E and Car R 2002 Theory of quantum annealing of an Ising spin glass *Science* **295** 2427–30
- [19] Roßnagel J, Dawkins S T, Tolazzi K N, Abah O, Lutz E, Schmidt-Kaler F and Singer K 2016 A single-atom heat engine *Science* **352** 325–9
- [20] Pekola J P 2015 Towards quantum thermodynamics in electronic circuits *Nat. Phys.* **11** 118
- [21] Doherty M W, Manson N B, Delaney P, Jelezko F, Wrachtrup J and Hollenberg L C L 2013 The nitrogen-vacancy colour centre in diamond *Phys. Rep.* **528** 1–45
- [22] Doherty M W, Dolde F, Fedder H, Jelezko F, Wrachtrup J, Manson N B and Hollenberg L C L 2012 Theory of the ground-state spin of the NV–center in diamond *Phys. Rev. B* **85** 205203
- [23] Bar-Gill N, Pham L M, Jarmola A, Budker D and Walsworth R L 2013 Solid-state electronic spin coherence time approaching one second *Nat. Commun.* **4** 1743
- [24] Häffner H, Roos C and Blatt R 2008 Quantum computing with trapped ions *Phys. Rep.* **469** 155–203
- [25] Kielpinski D, Monroe C and Wineland D J 2002 Architecture for a large-scale ion-trap quantum computer *Nature* **417** 709
- [26] Makhlin Y, Schön G and Shnirman A 2001 Quantum-state engineering with josephson-junction devices *Rev. Mod. Phys.* **73** 357
- [27] Martinis J M, Nam S, Aumentado J and Urbina C 2002 Rabi oscillations in a large josephson-junction qubit *Phys. Rev. Lett.* **89** 117901
- [28] Svetitsky E, Suchowski H, Resh R, Shalibo Y, Martinis J M and Katz N 2014 Hidden two-qubit dynamics of a four-level josephson circuit *Nat. Commun.* **5** 5617
- [29] Koch C P 2016 Controlling open quantum systems: tools, achievements, and limitations *J. Phys.: Condens. Matter.* **28** 213001
- [30] d'Alessandro D 2007 *Introduction to Quantum Control and Dynamics* (London: Chapman and Hall)
- [31] Constantin B, Chakrabarti R and Rabitz H 2010 Control of quantum phenomena: past, present and future *New J. Phys.* **12** 075008
- [32] Huang G M, Tarn T J and Clark J W 1983 On the controllability of quantum-mechanical systems *J. Math. Phys.* **24** 2608–18
- [33] Jurdjevic V and Sussmann H J 1972 Control systems on lie groups *J. Differ. Equ.* **12** 313–29
- [34] Ramakrishna V and Rabitz H 1996 Relation between quantum computing and quantum controllability *Phys. Rev. A* **54** 1715
- [35] Kosloff R, Rice S A, Gaspard P, Tersigni S and Tannor D J 1989 Wavepacket dancing: achieving chemical selectivity by shaping light pulses *Chem. Phys.* **139** 201–20
- [36] Zhu W and Rabitz H 1998 A rapid monotonically convergent iteration algorithm for quantum optimal control over the expectation value of a positive definite operator *J. Chem. Phys.* **109** 385–91
- [37] Palao J P and Kosloff R 2002 Quantum computing by an optimal control algorithm for unitary transformations *Phys. Rev. Lett.* **89** 188301
- [38] Machnes S, Sander U, Glaser S J, De Fouquières P, Gruslys A, Schirmer S and Schulte-Herbrüggen T 2011 Comparing, optimizing, and benchmarking quantum-control algorithms in a unifying programming framework *Phys. Rev. A* **84** 022305
- [39] Vitanov N V, Rangelov A A, Shore B W and Bergmann K 2017 Stimulated Raman adiabatic passage in physics, chemistry, and beyond *Rev. Mod. Phys.* **89** 015006
- [40] Albash T and Lidar D A 2018 Adiabatic quantum computation *Rev. Mod. Phys.* **90** 015002
- [41] Born M and Fock V 1928 Beweis des adiabatenatzes *Z. Phys.* **51** 165–80
- [42] Comparat D 2009 General conditions for quantum adiabatic evolution *Phys. Rev. A* **80** 012106
- [43] Dann R and Kosloff R 2021 Inertial theorem: overcoming the quantum adiabatic limit *Phys. Rev. Res.* **3** 013064
- [44] Schiff L I 1968 *Quantum Mechanics* 3rd edn (New York: McGraw-Hill) pp 61–2
- [45] Brown L S 1991 Quantum motion in a Paul trap *Phys. Rev. Lett.* **66** 527
- [46] Messiah A 1962 *Quantum Mechanics* vol 2 (Amsterdam: North-Holland)
- [47] Mostafazadeh A 1997 Quantum adiabatic approximation and the geometric phase *Phys. Rev. A* **55** 1653
- [48] Sarandy M S and Lidar D A 2005 Adiabatic approximation in open quantum systems *Phys. Rev. A* **71** 012331
- [49] Kato T 1950 On the adiabatic theorem of quantum mechanics *J. Phys. Soc. Japan* **5** 435–9
- [50] Fano U 1957 Description of states in quantum mechanics by density matrix and operator techniques *Rev. Mod. Phys.* **29** 74
- [51] Von Neumann J 2018 *Mathematical Foundations of Quantum Mechanics* New Edition (Princeton, NJ: Princeton University Press)
- [52] Gilmore R 2012 *Lie Groups, Lie Algebras, and Some of Their Applications* (Courier Corporation)

- [53] Alhassid Y and Levine R D 1978 Connection between the maximal entropy and the scattering theoretic analyses of collision processes *Phys. Rev. A* **18** 89
- [54] Dann R and Kosloff R 2020 Thermodynamically consistent dynamics of driven open quantum systems: from an autonomous framework to the semi-classical description (arXiv:2012.07979)
- [55] Leibfried D, Blatt R, Monroe C and Wineland D 2003 Quantum dynamics of single trapped ions *Rev. Mod. Phys.* **75** 281–324
- [56] Wineland D J, Monroe C, Itano W M, Leibfried D, King B E and Meekhof D M 1998 Experimental issues in coherent quantum-state manipulation of trapped atomic ions *J. Res. Natl Inst. Stand. Technol.* **103** 259
- [57] Hu C-K, Cui J-M, Santos A C, Huang Y-F, Sarandy M S, Li C-F and Guo G-C 2018 Experimental implementation of generalized transitionless quantum driving *Opt. Lett.* **43** 3136–9
- [58] Hu C-K, Cui J-M, Santos A C, Huang Y-F, Li C-F, Guo G-C, Brito F and Sarandy M S 2019 Validation of quantum adiabaticity through non-inertial frames and its trapped-ion realization *Sci Rep.* **9** 10449
- [59] Olmschenk S, Younge K C, Moehring D L, Matsukevich D N, Maunz P and Monroe C 2007 Manipulation and detection of a trapped Yb^+ hyperfine qubit *Phys. Rev. A* **76** 052314
- [60] Hu C-K, Santos A C, Cui J-M, Huang Y-F, Soares-Pinto D O, Sarandy M S, Li C-F and Guo G-C 2020 Quantum thermodynamics in adiabatic open systems and its trapped-ion experimental realization *Npj Quantum Inf.* **6** 73
- [61] Suzuki M 1976 Generalized Trotter's formula and systematic approximants of exponential operators and inner derivations with applications to many-body problems *Commun. Math. Phys.* **51** 183–90
- [62] Agarwal G S 1978 Quantum statistical theory of optical-resonance phenomena in fluctuating laser fields *Phys. Rev. A* **18** 1490–506
- [63] Gorini V, Kossakowski A and Sudarshan E C G 1976 Completely positive dynamical semigroups of n-level systems *J. Math. Phys.* **17** 821–5
- [64] Kosloff R and Feldmann T 2010 Optimal performance of reciprocating demagnetization quantum refrigerators *Phys. Rev. E* **82** 011134
- [65] Childs A M, Farhi E and Preskill J 2001 Robustness of adiabatic quantum computation *Phys. Rev. A* **65** 012322
- [66] Helstrom C W and Helstrom C W 1976 *Quantum Detection and Estimation Theory* vol 84 (New York: Academic)
- [67] Dann R, Levy A and Kosloff R 2018 Time-dependent markovian quantum master equation *Phys. Rev. A* **98** 052129
- [68] Dann R, Tobalina A and Kosloff R 2019 Shortcut to equilibration of an open quantum system *Phys. Rev. Lett.* **122** 250402
- [69] Dann R, Kosloff R and Salamon P 2020 Quantum finite-time thermodynamics: insight from a single qubit engine *Entropy* **22** 1255
- [70] Aharonov D, Van Dam W, Kempe J, Landau Z, Lloyd S and Regev O 2008 Adiabatic quantum computation is equivalent to standard quantum computation *SIAM Rev.* **50** 755–87
- [71] Farhi E, Goldstone J, Gutmann S and Sipser M 2000 Quantum computation by adiabatic evolution (arXiv:quant-ph/0001106)
- [72] Farhi E, Goldstone J, Gutmann S, Lapan J, Lundgren A and Preda D 2001 A quantum adiabatic evolution algorithm applied to random instances of an np-complete problem *Science* **292** 472–5
- [73] Perdomo-Ortiz A, Fluegemann J, Narasimhan S, Biswas R and Smelyanskiy V N 2015 A quantum annealing approach for fault detection and diagnosis of graph-based systems *Eur. Phys. J. Spec. Top.* **224** 131–48